Rotary Actuators with Electrostatic Suspension

Jong Up Jeon
Kanagawa Academy of Science and Technology
East Block 405, KSP, 3-2-1 Sakado, Takatsu-ku, Kawasaki 213, Japan
tel:+81-44-819-2093; fax:+81-44-819-2095; e-mail:jeon%naeba@intellect.pe.u-tokyo.ac.jp

Ju Jin
Kanagawa Academy of Science and Technology
East Block 405, KSP, 3-2-1 Sakado, Takatsu-ku, Kawasaki 213, Japan
tel:+81-44-819-2093; fax:+81-44-819-2095; e-mail:jujin@net.ksp.or.jp

Toshiro Higuchi
Dept. of Precision Machinery Eng., The University of Tokyo
7-3-1 Hongo, Bunkyo-ku, Tokyo 113, Japan
tel:+81-3-3812-2111 ext. 6449; fax:+81-3-5800-6968; e-mail:higuchi@intellect.pe.u-tokyo.ac.jp

Abstract: This paper studies two types of electrostatically suspended rotary actuators: electrostatically suspended variable-capacitance motors (ESVCM) and electrostatically suspended induction motors (ESIM). The ESVCM is an electrostatic stepping motor which features electrostatic suspension. Thus, ESVCM possesses the rotating and positioning ability of an ordinary stepping motor, in addition to providing contactless support by electrostatic suspension. To accomplish these two functions, a feedback control strategy and the operating principle of an ordinary electrostatic variable-capacitance motor are used. The ESIM is an induction motor where the rotor is suspended stably, like ESVCM, by actively controlling the electrostatic forces exerted on it. To implement a rotation, the operating principle of an ordinary electrostatic induction motor is used.

In this paper, the working principle of the ESVCM and the ESIM, electrode design, a linear dynamic model of the suspension system, feedback control strategy and operating principle of rotation are described. Experimental results show that the rotor has been rotated with a speed of approximately 60 rpm while being suspended stably at a gap length of 300 μm.

1 Introduction

Magnetically suspended stepping actuators for use in ultra-high-vacuum (UHV) and clean-room environments have already been studied [1]. However, these actuators can not handle non-ferromagnetic materials directly since a magnetic force can not exert forces on it. Therefore, in order to manipulate a non-ferromagnetic object, additional devices to support it are needed, which leads to direct mechanical contact and consequently generation of particles. On the other hand, in the manufacturing process for liquid crystal displays (LCD), the handling of a glass plate by mechanical contact is becoming more critical since its thickness/surfacial area ratio is becoming smaller. Thus, glass plate handling systems without any physical contact are indispensable. It is apparent that electromagnetic forces can not be utilized since glass is not a ferromagnetic material. Electrostatic suspension has the potential to remedy the above problem.

Electrostatic levitation has several novel advantages compared to electromagnetic levitation. The advantage of using electric forces is that very high energy densities can be achieved in the very small scale involved [2]. In the micro electro mechanical field, electrostatic suspension has been experimentally studied to eliminate the friction and physical contact [3]. Electrostatic levitation also offers the advantage to directly levitate various materials such as conductive materials, semiconductors and dielectric materials. The authors have already succeeded in directly suspending a silicon wafer using electrostatic forces [4]. This paper reports about the successful suspension and rotation of a glass disk by electrostatic forces.

Like electromagnetic motors, electrostatic motors can be classified as synchronous or asynchronous. The variable-capacitance motor which is synchronous has received much attention to date due to its simplicity [5][6]. An induction motor which is asynchronous has been developed by Bollee[5] and by Choi *et al.* [7]. In their research, rotors made of a slightly conductive material, such as Bakelite and Plexiglas [7] and glass covered with a layer of resistive material [5], were utilized. However, these types of motors use bushing to support the rotor and therefore can not be used in UHV and clean environments since the mechanical wear occurring in the bushing will generate particles. Consequently, to implement contactless and friction-free handling devices for non-ferromagnetic materials such as silicon wafers and glass, a function of suspension has to be incorporated in addition to an actuating function.

In this paper, we propose two types of electrostatically suspended rotary actuators (ESRA): electrostatically suspended variable-capacitance motors (ESVCM) and electrostatically suspended induction motors (ESIM). The ESRA is a rotary actuator that possesses the function of electrostatic levitation. In ESRA, the rotor is supported by electrostatic forces without any physical contact with the environment and therefore the generation of particles can be eliminated.

2 Electrostatically Suspended Variable-Capacitance Motors (ESVCM)

2.1 Principle of ESVCM

The ESVCM is a variable-capacitance stepping motor which includes the function of contactless electrostatic suspension.

To implement a stable suspension, we need to exert forces along five axes excluding the rotational axis. By locating the

stator electrodes above the rotor, electrostatic forces to control the vertical movement(z), pitching(θ) and rolling(ψ) can be generated. However, since these electrostatic forces destabilize the system, stabilization has to be achieved by actively controlling these attractive forces. The non-actively controlled movements in the horizontal plane of the rotor, are passively stabilized through a restriction force that originates from a relative lateral translation of the rotor with respect to the stator electrodes [8].

Similar to ordinary electrostatic variable-capacitance motors, the operational principle of rotation in ESVCM is based on the variation of the capacitance between the stator and rotor with the rotation of the rotor. Thus, both the stator and rotor in ESVCM possess a number of teeth while the teeth distribution of the stator electrodes is different from that of the rotor electrodes.

2.2 Electrode Design for Stator and Rotor

Fig. 1 depicts the electrode pattern of the stator and rotor in

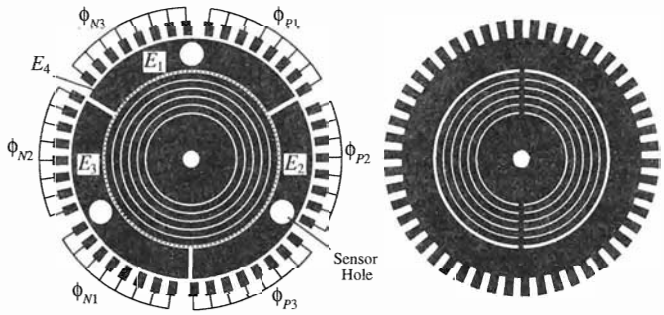

Fig. 1 Electrode pattern of stator and rotor in ESVCM

ESVCM. The stator electrodes comprise two functionally distinct parts. The central area is used for stable suspension of the rotor and the peripheral area is used for the generation of a torque to rotate it. The suspension area is subdivided into four sections (denoted as E_j, where j=1,2,3,4), each of which act as independent actuators of force on the rotor. Among them, the outer three electrodes E_1, E_2 and E_3, which together form a ring, have the same shape and area. To increase the lateral restorative forces, which help to improve rotational performance of ESVCM, ring shape slits are formed in the section E_4 and the corresponding part of the rotor. The area of electrode E_4 is three times that of E_1. For the purpose of measuring the gap length between each electrode E_i (i=1,2,3) and the rotor, each individual electrode is supplied with a contactless gap sensor.

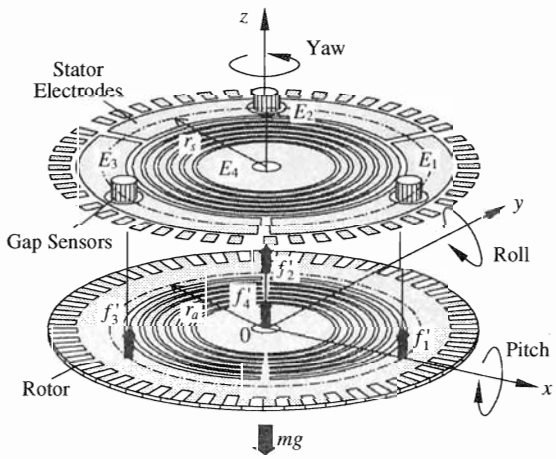

Fig. 2 Coordinate system and definition of terminology in ESVCM

The outer region of the stator electrode consists of six sets of teeth, denoted by ϕ_{Pi} and ϕ_{Ni}, where i=1,2,3. Each ϕ_{Pi} and ϕ_{Ni} pair form one phase. In the stator, the teeth of each set has the same tooth pitch as that of the rotor, and each set is displaced by 1/3 of a single tooth pitch from phase to phase. Thus, the electrodes-for-rotation, basically, form a similar structure to that of three-phase variable-capacitance motors.

2.3 Dynamic Model for Suspension

2.3.1 *Nonlinear Equation of Motion for Suspension*

In the following analysis, concerning the variables to be linearized around the nominal operating points, the superscript "'" denotes the total value, and the subscript "0" denotes the value at the equilibrium state. Symbols without superscript "'" and subscript "0" are small variable terms from the equilibrium state.

Fig. 2 shows a simplified representation of the experimental system which defines the coordinate system and terminology to be used in our analysis. We define a reference coordinate frame $\Sigma(O\text{-}xyz)$ so that in state of no rotation, when the rotational axis of the rotor coincides with the center line of the electrodes, the origin O is located at the rotor's center of mass and the z axis is coincident with the rotational axis. Each of the distributed forces generated by the four electrodes-for-suspension can be treated as an equivalent concentrated force with its point of application at the geometrical center of the electrode.

As mentioned previously, three of the five degrees of freedom of the rotor are actively controlled: movement in vertical direction, pitching and rolling. Assuming that the rotor is a floating rigid body and the rotor movement is very small, the fundamental equations of motion of the rotor for the three degrees-of-freedom are as follows

$$\begin{aligned} m\ddot{z}' &= f_1' + f_2' + f_3' + f_4' + f_{ez}' \\ J_r\ddot{\theta}' &= \frac{\sqrt{3}r_a}{2}\left(f_2' - f_3'\right) + f_{e\theta}' \\ J_r\ddot{\psi}' &= \frac{r_a}{2}\left(-2f_1' + f_2' + f_3'\right) + f_{e\psi}' \end{aligned} \tag{1}$$

where m is the mass of the rotor, J_r is the moment of inertia in lateral direction, r_a is the distance between the geometrical centers of the electrodes-for-suspension E_i (i=1,2,3) and the origin O, z' is the z-coordinate of the rotor's center of mass, (θ', ψ') are the angular displacements of the rotational axis about the x- and y-axis respectively, f_1',f_2',f_3',f_4' are the electrostatic forces produced by the stator electrodes-for-suspension, and f_{ez}',$f_{e\theta}'$,$f_{e\psi}'$ are the external forces including the weight of the rotor and the electrostatic forces produced by the electrodes-for-rotation. Note that the gyroscopic effects can be neglected since the rotor speed in ESVCM is relatively low.

Let $\boldsymbol{r}'=(z', \theta', \psi')^{\mathrm{T}}$, $\boldsymbol{M}=\mathrm{diag}(m, J_r, J_r)$, $\boldsymbol{f}'^4=(f_1', f_2', f_3', f_4')^{\mathrm{T}}$, $\boldsymbol{f}_e'=(f_{ez}', f_{e\theta}', f_{e\psi}')^{\mathrm{T}}$. Using vector notation, the nonlinear equa-

tion of motion (1) can be rewritten as follows

$$\ddot{\boldsymbol{r}}' = \boldsymbol{M}^{-1}\boldsymbol{T}_a\boldsymbol{f}'^4 + \boldsymbol{M}^{-1}\boldsymbol{f}_e' \tag{2}$$

where $\boldsymbol{T}_a$ is the location matrix of the electrodes-for-suspension and is given by

$$\boldsymbol{T}_a = \begin{bmatrix} 1 & 1 & 1 & 1 \\ 0 & \frac{\sqrt{3}}{2}r_a & -\frac{\sqrt{3}}{2}r_a & 0 \\ -r_a & \frac{r_a}{2} & \frac{r_a}{2} & 0 \end{bmatrix} \tag{3}$$

2.3.2 *Electrostatic Force*

When the overlapping area A_j of an electrode-for-suspension j and the rotor is large enough compared with the gap length d_j', the capacitance C_j' can be approximated as

$$C_j' = \frac{\varepsilon A_j}{d_j'}, \quad j = 1, 2, 3, 4 \tag{4}$$

The electrostatic force f_j' can be expressed in terms of the gap length d_j', the voltage V_j' supplied to the j'th electrode, and the rotor potential V_f'

$$f_j' = \frac{\varepsilon A_j}{2}\left(\frac{V_j' - V_f'}{d_j'}\right)^2, \quad j = 1, 2, 3, 4 \tag{5}$$

where ε denotes the permittivity. For the computation of f_j', it is imperative to know V_f' as a function of the voltages V_j' and the capacitances C_j'. Note that the capacitance C_j' is a function of gap length d_j' as shown in (4). Fig. 3 shows a diagram which

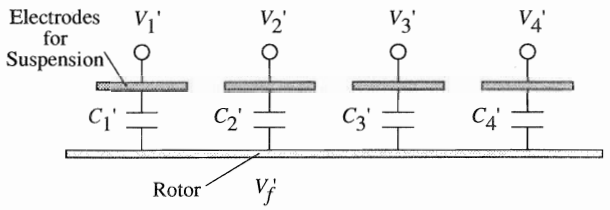

Fig. 3 Equivalent circuit of electrode-for-suspension array -rotor configuration in ESVCM

represents an equivalent circuit of the electrode-for-suspension array-rotor configuration, where only the capacitances C_j' are considered as impedance elements. Using Kirchhof's law, the rotor potential V_f' can be derived as

$$V_f' = \frac{\sum_{k=1}^{4}(C_k'V_k')}{\sum_{k=1}^{4}C_k'} \tag{6}$$

From (4), (5) and (6), the electrostatic force f_j' can be calculated. Note that the electrostatic forces f_j's are coupled due to the fact that V_f' is a function of the voltages V_1', V_2', V_3', V_4' and the capacitances C_1', C_2', C_3', C_4'. In order to decouple each f_j', which results in a decoupling of each degree of freedom, a necessary condition is that V_f' has to be kept to zero voltage. From (6), the potential V_f' can be zero if the voltage V_4' is chosen as follows

$$V_4' = -\frac{\sum_{k=1}^{3}(C_k'V_k')}{C_4'} \tag{7}$$

In the following analysis, the rotor potential is assumed to be zero because the voltage of electrode #4 will be controlled to satisfy the condition (7).

Under the condition (7), the force f_4' can be represented as a function of f_1', f_2', and f_3'. From (4), (5), (7) and (8), and by considering the geometrical conditions $A_1=A_2=A_3=A_4/3=A$ and

$$d_4' = \frac{d_1' + d_2' + d_3'}{3} \tag{8}$$

the electrostatic force f_4' can be expressed as

$$f_4' = \frac{1}{3}\left(\sqrt{f_1'} + \sqrt{f_2'} + \sqrt{f_3'}\right)^2 \tag{9}$$

2.3.3 *Linearized Equation of Motion*

The nonlinear equation of motion (2) is linearized around the nominal operating point under the assumption that the deviations from the nominal values are very small. If we linearize the electrostatic forces, then we can write

$$f_i' = f_{0i} + f_i, \; f_4' = f_{04} + f_4, \; V_i' = V_{0i} + V_i, \; d_i' = d_{0i} + d_i, \quad i = 1, 2, 3$$

where $$f_{0i} = \frac{\varepsilon A}{2}\left(\frac{V_{0i}}{d_{0i}}\right)^2, \; f_{04} = \frac{1}{3}\left(\sqrt{f_{01}} + \sqrt{f_{02}} + \sqrt{f_{03}}\right)^2,$$

$$f_i = k_{Vi}V_i - k_{si}d_i, \; f_4 = f_1 + f_2 + f_3 \tag{10}$$

and k_{si} and k_{Vi} are the linearization constants given by

$$k_{si} = \frac{\varepsilon A V_{0i}^2}{d_{0i}^3}, \; k_{Vi} = \frac{\varepsilon A V_{0i}}{d_{0i}^2} \tag{11}$$

Let $\boldsymbol{r}_0=(z_0, \theta_0, \psi_0)^{\mathrm{T}}$, $\boldsymbol{r}=(z, \theta, \psi)^{\mathrm{T}}$, $\boldsymbol{f}_0{}^4=(f_{01}, f_{02}, f_{03}, f_{04})^{\mathrm{T}}$, $\boldsymbol{f}^4=(f_1, f_2, f_3, f_4)^{\mathrm{T}}$, $\boldsymbol{f}_{e0}=(f_{e0z}, f_{e0\theta}, f_{e0\psi})^{\mathrm{T}}$, $\boldsymbol{f}_e=(f_{ez}, f_{e\theta}, f_{e\psi})^{\mathrm{T}}$. By defining $\boldsymbol{r}'=\boldsymbol{r}_0+\boldsymbol{r}$, $\boldsymbol{f}'^4=\boldsymbol{f}_0{}^4+\boldsymbol{f}^4$ and $\boldsymbol{f}_e'=\boldsymbol{f}_{e0}+\boldsymbol{f}_e$, the equation of motion (2) can be rewritten as

$$\ddot{\boldsymbol{r}}_0 + \ddot{\boldsymbol{r}} = \boldsymbol{M}^{-1}\boldsymbol{T}_a\boldsymbol{f}_0^4 + \boldsymbol{M}^{-1}\boldsymbol{T}_a\boldsymbol{f}^4 + \boldsymbol{M}^{-1}\boldsymbol{f}_{e0} + \boldsymbol{M}^{-1}\boldsymbol{f}_e \tag{12}$$

From the above equation, the nominal operating voltage V_{0j} can be selected to satisfy the following equation

$$\boldsymbol{T}_a\boldsymbol{f}_0^4 + \boldsymbol{f}_{e0} = \boldsymbol{0} \quad (\ddot{\boldsymbol{r}}_0 = \boldsymbol{0}) \tag{13}$$

Substracting (13) from (12), the linearized dynamic equation of motion of the rotor becomes

$$\ddot{\boldsymbol{r}} = \boldsymbol{M}^{-1}\boldsymbol{T}_a\boldsymbol{f}^4 + \boldsymbol{M}^{-1}\boldsymbol{f}_e \tag{14}$$

If we define a vector $\boldsymbol{f}$ as $\boldsymbol{f}=(f_1, f_2, f_3)^{\mathrm{T}}$, $\boldsymbol{f}^4$ can be transformed to $\boldsymbol{f}$ through the transformation matrix $\boldsymbol{T}_4$ as follows

$$\boldsymbol{f}^4 = \boldsymbol{T}_4\boldsymbol{f}$$

where $$\boldsymbol{T}_4 = \begin{bmatrix} 1 & 0 & 0 & 1 \\ 0 & 1 & 0 & 1 \\ 0 & 0 & 1 & 1 \end{bmatrix}^{\mathrm{T}} \tag{15}$$

Let $\boldsymbol{d}=(d_1, d_2, d_3)^{\mathrm{T}}$. By considering the geometrical condition between $\boldsymbol{d}$ and $\boldsymbol{r}$, $\boldsymbol{d}$ can be transformed to $\boldsymbol{r}$ as

$$\boldsymbol{d} = -\boldsymbol{T}_d\boldsymbol{r}, \quad \boldsymbol{T}_d = \begin{bmatrix} 1 & 0 & -r_a \\ 1 & \frac{\sqrt{3}r_a}{2} & \frac{r_a}{2} \\ 1 & -\frac{\sqrt{3}r_a}{2} & \frac{r_a}{2} \end{bmatrix} \tag{16}$$

From (10), (14), (15) and (16), the linearized dynamic equation of motion of the rotor becomes

$$\ddot{\boldsymbol{r}} = \boldsymbol{M}^{-1}\boldsymbol{T}_a\boldsymbol{T}_4\boldsymbol{K}_s\boldsymbol{T}_d\boldsymbol{r} + \boldsymbol{M}^{-1}\boldsymbol{T}_a\boldsymbol{T}_4\boldsymbol{K}_V\boldsymbol{V} \tag{17}$$

where $\boldsymbol{V}=(V_1, V_2, V_3)^{\mathrm{T}}$, $\boldsymbol{K}_s=\mathrm{diag}(k_{s1}, k_{s2}, k_{s3})$ and $\boldsymbol{K}_V=\mathrm{diag}(k_{V1}, k_{V2}, k_{V3})$. Note that in (17), the variable term of the external force, $\boldsymbol{f}_e$, which mainly originates from the electrostatic forces produced by the electrodes-for-rotation, is neglected since it is much smaller than the forces produced by the electrodes-for-suspension.

In order to decouple each degree of freedom, the matrix $\boldsymbol{T}_a\boldsymbol{T}_4\boldsymbol{K}_s\boldsymbol{T}_d$ should be diagonal, which is accomplished for $k_{s1}=k_{s2}=k_{s3}$. In this case, from (11) and (13), we find that all the nominal gap lengths d_{0i} and all the nominal operating voltages V_{0i}, where $i=1,2,3$, are equal. Let $k_{s1}=k_{s2}=k_{s3}=k_s$, $k_{V1}=k_{V2}=k_{V3}=k_V$ and $\boldsymbol{T}_a\boldsymbol{T}_4\boldsymbol{T}_d=\boldsymbol{Q}_r$, where $\boldsymbol{Q}_r$ is a diagonal matrix. Then the linearized dynamic equation of motion of the rotor is rewritten as

$$\ddot{\boldsymbol{r}} = k_s\boldsymbol{M}^{-1}\boldsymbol{Q}_r\boldsymbol{r} + k_V\boldsymbol{M}^{-1}\boldsymbol{T}_a\boldsymbol{T}_4\boldsymbol{V} \tag{18}$$

From the above equation (18), we can observe the unstable open-loop dynamics of the rotor which necessitates the utilization of feedback control for stabilization.

2.4 Stabilizing Controller for Suspension

To stabilize the motion of the rotor, the feedback controller is designed on the basis of the position vector $\boldsymbol{r}$. Let $\boldsymbol{V}_r$, $\boldsymbol{P}_d$, $\boldsymbol{P}_v$ and $\boldsymbol{P}_I$ be the feedback control voltage vector, proportional, derivative and integral gain matrices which are defined by $\boldsymbol{V}_r=(V_z, V_\theta, V_\psi)^{\mathrm{T}}$, $\boldsymbol{P}_d=\mathrm{diag}(p_{dz}, p_{d\theta}, p_{d\psi})$, $\boldsymbol{P}_v=\mathrm{diag}(p_{vz}, p_{v\theta}, p_{v\psi})$, $\boldsymbol{P}_I=\mathrm{diag}(p_{Iz}, p_{I\theta}, p_{I\psi})$, respectively. Then $\boldsymbol{V}_r$ is determined as

$$\boldsymbol{V}_r = -\left(\boldsymbol{P}_d\boldsymbol{r} + \boldsymbol{P}_v\dot{\boldsymbol{r}} + \boldsymbol{P}_I\int \boldsymbol{r}dt\right) \tag{19}$$

To obtain the control voltage $\boldsymbol{V}$, $\boldsymbol{V}_r$ is transformed to $\boldsymbol{V}$ using a pre-compensation matrix $\boldsymbol{T}_V$ as follows

$$\boldsymbol{V} = \boldsymbol{T}_V\boldsymbol{V}_r \tag{20}$$

Inserting (20) into (18), the linearized equation of motion of the rotor is given by

$$\ddot{\boldsymbol{r}} = k_s\boldsymbol{M}^{-1}\boldsymbol{Q}_r\boldsymbol{r} + k_V\boldsymbol{M}^{-1}\boldsymbol{T}_a\boldsymbol{T}_4\boldsymbol{T}_V\boldsymbol{V}_r \tag{21}$$

Here, $\boldsymbol{T}_V$ can be determined in order to decouple each degree of freedom. To achieve this, $\boldsymbol{T}_a\boldsymbol{T}_4\boldsymbol{T}_V$ should satisfy the following relation

$$\boldsymbol{T}_a\boldsymbol{T}_4\boldsymbol{T}_V = \boldsymbol{Q}_V \tag{22}$$

where $\boldsymbol{Q}_V$ is a diagonal matrix and is defined by $\boldsymbol{Q}_V=\mathrm{diag}(q_{V1}, q_{V2}, q_{V3})$. From (19), (21) and (22), the closed-loop rotor dynamics becomes

$$\begin{aligned}\ddot{\boldsymbol{r}} + k_V\boldsymbol{M}^{-1}\boldsymbol{Q}_V\boldsymbol{P}_v\dot{\boldsymbol{r}} + (k_V\boldsymbol{M}^{-1}\boldsymbol{Q}_V\boldsymbol{P}_d - k_s\boldsymbol{M}^{-1}\boldsymbol{Q}_r)\,\boldsymbol{r} \\ + k_V\boldsymbol{M}^{-1}\boldsymbol{Q}_V\boldsymbol{P}_I\int \boldsymbol{r}dt = \boldsymbol{0}\end{aligned} \tag{23}$$

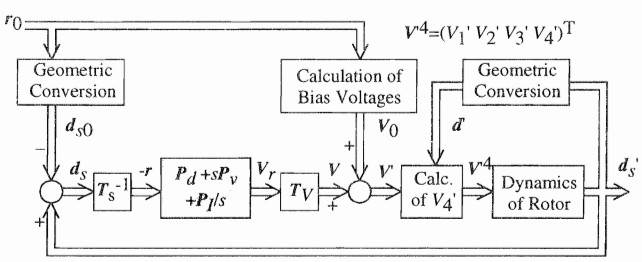

Fig. 4 Block diagram of closed-loop control system

It is apparent that with a proper choice of $\boldsymbol{P}_d$, $\boldsymbol{P}_v$, $\boldsymbol{P}_I$ and $\boldsymbol{Q}_V$, this system can be stabilized.

In order to obtain $\boldsymbol{V}_r$ on the basis of (19), $\boldsymbol{r}$ should be known. Let $\boldsymbol{d}_s=(d_{s1}, d_{s2}, d_{s3})$ be the displacement vector which contains the outputs of the three gap sensors and is defined by $\boldsymbol{d}_s=\boldsymbol{d}_s'-\boldsymbol{d}_{s0}$. The following geometric relation between $\boldsymbol{r}$ and $\boldsymbol{d}_s$ can be obtained

$$\boldsymbol{d}_s = -\boldsymbol{T}_s\boldsymbol{r}, \quad \boldsymbol{T}_s = \begin{bmatrix} 1 & 0 & -r_s \\ 1 & \frac{\sqrt{3}r_s}{2} & \frac{r_s}{2} \\ 1 & -\frac{\sqrt{3}r_s}{2} & \frac{r_s}{2} \end{bmatrix} \tag{24}$$

From the above equation, $\boldsymbol{r}$ can be solved as

$$\boldsymbol{r} = -\boldsymbol{T}_s^{-1}\boldsymbol{d}_s \tag{25}$$

To obtain $\boldsymbol{V}$ from (20), the matrix $\boldsymbol{T}_V$ should be known. By solving (22) for $\boldsymbol{T}_V$, we obtain

$$\boldsymbol{T}_V = (\boldsymbol{T}_a\boldsymbol{T}_4)^{-1}\boldsymbol{Q}_V = \frac{1}{3}\begin{bmatrix} \frac{q_{V1}}{2} & 0 & -\frac{2q_{V3}}{r_a} \\ \frac{q_{V1}}{2} & \frac{\sqrt{3}q_{V2}}{r_a} & \frac{q_{V3}}{r_a} \\ \frac{q_{V1}}{2} & -\frac{\sqrt{3}q_{V2}}{r_a} & \frac{q_{V3}}{r_a} \end{bmatrix} \tag{26}$$

The block diagram of the closed-loop control system is shown in Fig. 4.

When implementing the controller, it is convenient to know the relation between $\boldsymbol{d}_s$ and $\boldsymbol{V}$. From (19), (20) and (25), we can obtain the following relation

$$\boldsymbol{V} = \boldsymbol{P}_{dS}\boldsymbol{d}_s + \boldsymbol{P}_{vS}\dot{\boldsymbol{d}}_s + \boldsymbol{P}_{IS}\int \boldsymbol{d}_s dt \tag{27}$$

where $\boldsymbol{P}_{dS}=\boldsymbol{T}_V\boldsymbol{P}_d\boldsymbol{T}_s^{-1}$, $\boldsymbol{P}_{vS}=\boldsymbol{T}_V\boldsymbol{P}_v\boldsymbol{T}_s^{-1}$ and $\boldsymbol{P}_{IS}=\boldsymbol{T}_V\boldsymbol{P}_I\boldsymbol{T}_s^{-1}$. Note that despite the decoupling between each degree of freedom, coupling between the components of $\boldsymbol{V}$ and $\boldsymbol{d}_s$ arises.

2.5 Operating Principle for Rotation

To realize rotations, dc voltages are supplied sequentially to each phase of the electrodes-for-rotation. If phase #1 is energized by applying dc voltages to the electrodes ϕ_{P1} and ϕ_{N1}, electrostatic forces will position the rotor in such a way that the rotor teeth under the excited phase #1 are lined up opposite the stator teeth of the same phase. Next, if the voltages are

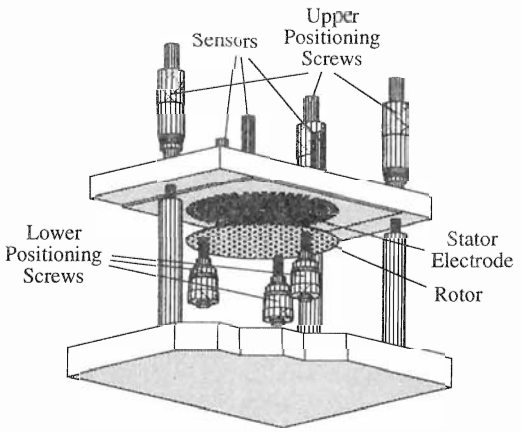

Fig. 5 Schematic diagram of experimental apparatus

switched from phase #1 to phase #2, the rotor will rotate by a single step angle and the rotor teeth will be aligned opposite the teeth of phase #2 of the stator. Continuing in the same way, the input sequence of 1231... will rotate the rotor counterclockwise. To rotate in the clockwise direction the sequence is reversed. Because a positive voltage is supplied to phase ϕ_{Pi} and a negative voltage to ϕ_{Ni}, where both voltages have the same magnitudes, the rotor potential is maintained at zero voltage, leading to a decoupling of each degree of freedom in the control system for suspension as described above.

2.6 Experimental Work and Results

2.6.1 *Experimental System Configuration*

Fig. 5 shows the schematic diagram of the experimental apparatus. The stator electrodes are etched from a 35 μm thick copper layer on a glass-epoxy base. The widths of the ring shape slits in E_4 is 1 mm. Electrodes #1, #2 and #3 have the same area of 7.6 cm^2 and the area of electrode #4 is three times that of electrode #1. The rotor electrode is etched in a similar manner to the stator on a 0.4 mm thick glass plate. The rotor has a diameter of 100 mm and a mass of 10.8 g. The teeth for rotation have a pitch of 7.2 degrees, a tooth width of 3.6 degrees, and a tooth length of 5 mm. Fig. 6 depicts a photograph

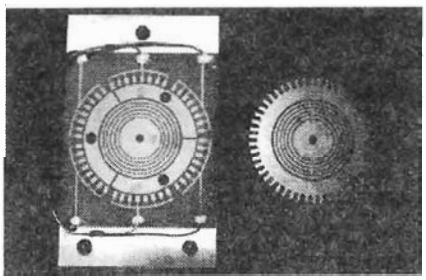

Fig. 6 Photograph of stator and rotor in ESVCM

of the stator and the rotor. Three eddy-current type gap sensors, positioned at the corners of an equilateral triangle which can be circumscribed by a circle of radius 38 mm, are employed to measure the stator-rotor gap lengths. By adjusting the heights of micrometer positioning screws, the stator electrode is leveled and the initial gap length is set.

Fig. 7 shows the block diagram of the control system. Voltages for suspension and those for rotation are controlled independently. In the control system for suspension, a limiting action is imposed on the voltages for suspension to prevent electric discharge which is caused by the breakdown of the electric field.

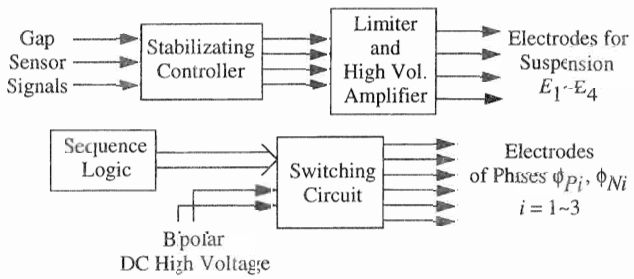

Fig. 7 Block diagram of control system in ESVCM

2.6.2 *Suspension Experiments*

Suspension experiments have been performed in an atmospheric environment. Proportional, derivative and integral gains for the vertical movement of the rotor are 10^5 kV/m, 50 kVsec/m and 10^6 kV/msec, respectively, and those for rolling and pitching are 55 kV/rad, 0.03 kVsec/rad and 10^4 kV/radsec, respectively. A bias voltage of 0.53 kV is supplied to electrode #1, #2 and #3, and -0.53 kV to electrode #4. Fig. 8 shows the

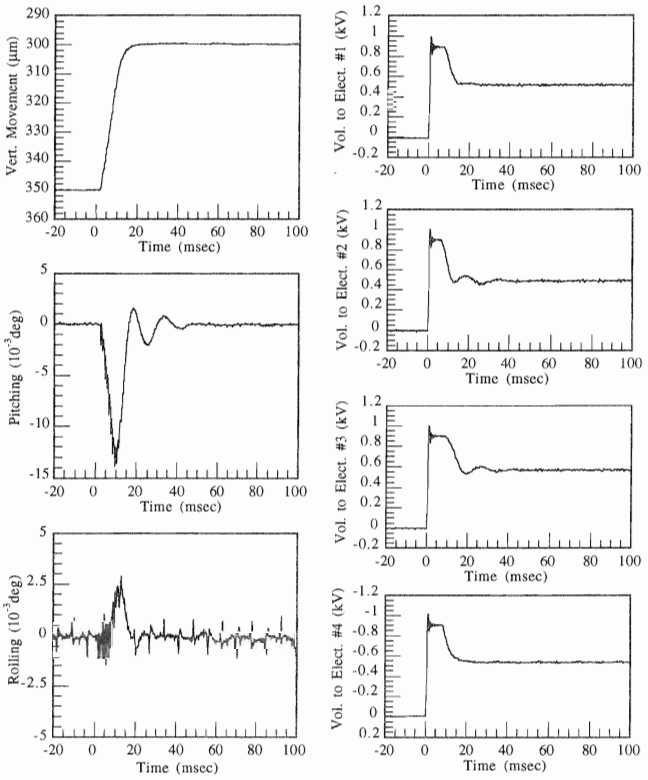

Fig. 8 Rotor position and voltage variations during levitation process in ESVCM

variations of the rotor position and orientation after the PID compensator was switched on. It can be observed that from the initial gap length 350 μm, the rotor is pulled up towards the stator reaching a stable state of suspension at a reference gap length of 300 μm in about 50 msec. Fig. 8 also shows the voltage variations during the picking up process of the rotor. It shows that when the rotor reached the stable levitation position, the voltages applied to the electrodes-for-suspension were respectively 0.52 kV, 0.49 kV, 0.57 kV and -0.53 kV.

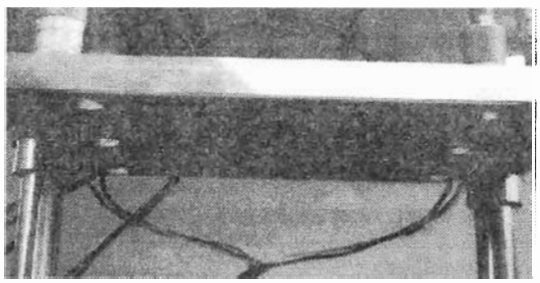

Fig. 9 Photograph showing rotor under stable suspension in ESVCM

Fig. 9 is a photograph which shows the rotor under stable suspension.

2.6.3 *Rotation Experiments*

To rotate the rotor, dc voltages of 0.7 kV and -0.7 kV were supplied sequentially to each phase of the electrodes-for-rotation after a stable levitation was achieved at a gap length of 300 μm. Fig. 10 shows a single step response of the rotor in 1-

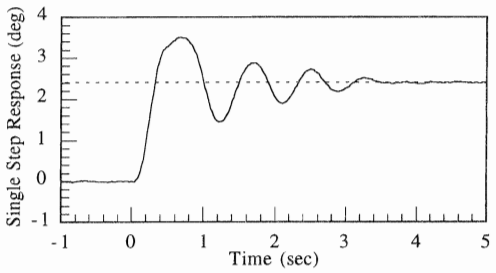

Fig. 10 Single step response in ESVCM

phase excitation. It shows that the positioning time of a single step angle of 2.4 degrees was about 3.5 seconds. The attainable maximum rotor speed was also investigated. It was observed that the main factor restricting the maximum speed is not the rotational torque but the passive lateral restriction force. When the rotor speed reached above 60 rpm, the movement of the rotor along lateral direction became unstable due to an insufficiency of the restorative forces. Concerning the attainable maximum acceleration, it was recorded that a time period of 10 seconds was required to raise the speed from 0 up to 60 rpm. Fig. 11 shows the variations of the gap lengths and the voltages supplied to the electrodes-for-suspension at a rotor

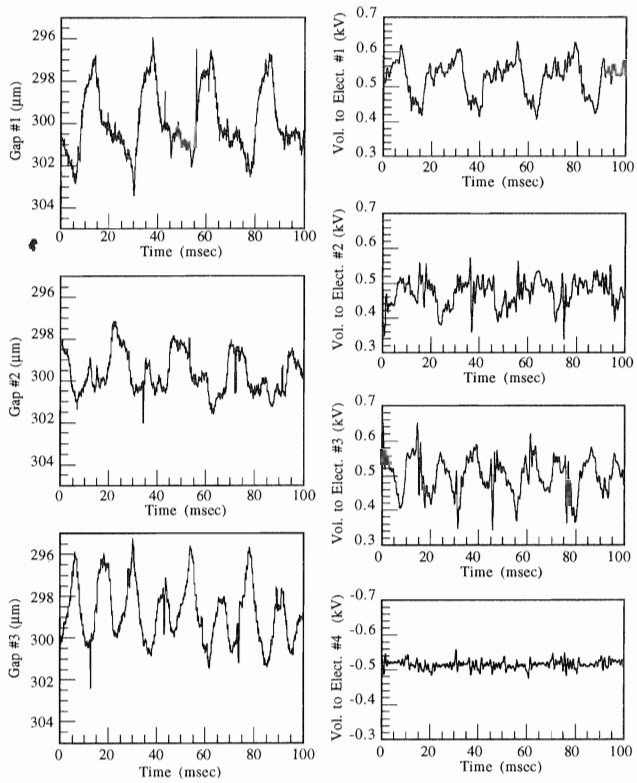

Fig. 11 Gap and voltage variations during rotation in ESVCM

speed of 50 rpm. The fluctuations of the gap lengths have been verified not to exceed 6 μm p-p while those of the voltages supplied to electrodes #1, #2, #3 and #4 did not exceed 0.2 kV, 0.18 kV, 0.22 kV, and 0.05 kV, respectively.

To explore the braking characteristics of the rotor, a retardation curve, as shown in Fig. 12, was measured. It was ob-

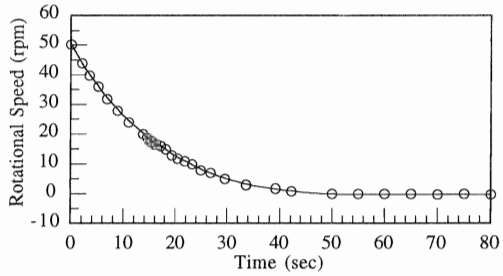

Fig. 12 Retardation curve of ESVCM

served that it took about 50 seconds for the rotor to stop it's rotation from an initial speed of 50 rpm.

3 Electrostatically Suspended Induction Motors (ESIM)

3.1 Principle of ESIM

The ESIM is an electrostatic induction motor where the rotor is supported by actively controlled electrostatic forces. The manner to realize a stable suspension of the rotor in ESIM is identical to that in ESVCM. The operating principle of rotation in ESIM, like ordinary electrostatic induction motors, is based on the fact that a rotor made of a material which is slightly electrically conducting (a "poor insulator") is subjected to a torque when placed in a rotating electric field. The explanation for this lies in the fact that the high resistivity causes the induced charges on the rotor surface to lag behind the rotating field. As a consequence, a torque will be exerted by the rotating field on those charges and hence on the rotor. In ESIM, the rotating electric field is generated by supplying ac voltages to a number of teeth formed on the stator. As rotor material, glass is employed which is slightly conductive.

3.2 Structure of ESIM and Control Strategy

Fig. 13 depicts the stator electrode pattern of ESIM, which

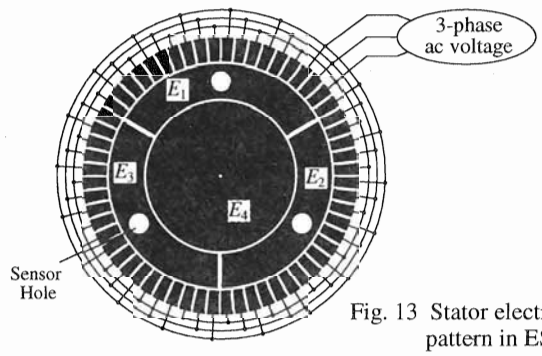

Fig. 13 Stator electrode pattern in ESIM

is similar to that of ESVCM. The central area of the stator electrodes is composed of the electrodes for stable suspension. The main difference between the structure of electrodes-for-suspension in ESIM and that in ESVCM is that the former

does not have any ring shape slits as in ESVCM. The outer region of the stator electrodes in ESIM consists of a number of teeth with an uniform tooth pitch along the circumference of the stator electrodes, and each tooth is connected to form three phases.

As a rotor, we utilized two types of rotors: a glass disk covered on only one side with a thin layer of conductive material (ITO layer), and a glass disk without any surface treatment.

The control strategy to stabilize the rotor suspension is the same as that of ESVCM. To generate a rotating electric field and consequently a rotational torque on the rotor, three-phase ac voltages which differ in phase by 120° are supplied to the electrodes-for-rotation.

3.3 Experimental Work and Results

3.3.1 *Experimental System Configuration*

The experimental apparatus of ESIM and the manufacturing method of stator electrodes are similar to those of ESVCM. Like ESVCM, electrodes #1, #2 and #3 have the same area of 7.6 cm^2 and the area of electrode #4 is three times that of electrode #1. Three fiber optical sensors are located at the corners of an equilateral triangle which can be circumscribed by a circle of radius 35 mm. The teeth for rotation have a pitch of 6 degrees, a tooth width of 3 degrees and a tooth length of 8 mm. Fig. 14 depicts a photograph of the stator. The glass disk has a

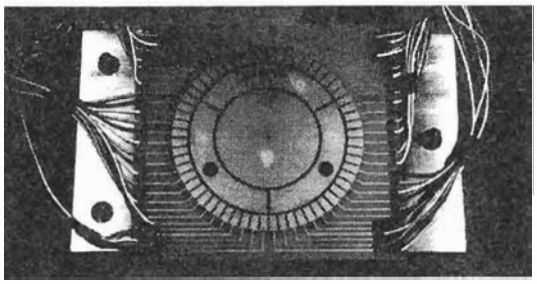

Fig. 14 Photograph of stator in ESIM

diameter of 100 mm, a thickness of 0.7 mm and a mass of 13.8 g. The surface resistivity and the volume resistivity of the glass disk were measured to be approximately $2 \cdot 10^{13}$ Ω and 10^{13} Ω/m, respectively, for an air humidity of 50 %RH and temperature of 25 °C, while the surface resistivity of the ITO layered disk was about 10^6 Ω. In case of the ITO layered glass disk, the side of the disk without ITO layer should be positioned to face the stator electrodes. Utilization of an ITO layer contributes to an improvement of the suspension stability, in particular along the lateral direction, which was verified experimentally.

3.3.2 *Experimental Results*

Prior to rotation, suspension experiments were carried out with the ITO layered glass disk in an atmospheric environment. The control gains were nearly the same as those of ESVCM. A bias voltage of 0.67 kV was supplied to electrode #1, #2 and #3, and -0.67 kV to electrode #4. It was observed that after switching on the PID compensator, the rotor was pulled up from an initial gap length of 350 μm and reached a stable state of suspension at a reference gap length of 300 μm. In this state, the voltages applied to the electrodes-for-suspension were respectively 0.72 kV, 0.62 kV, 0.7 kV and -0.68 kV. Fig. 15 is

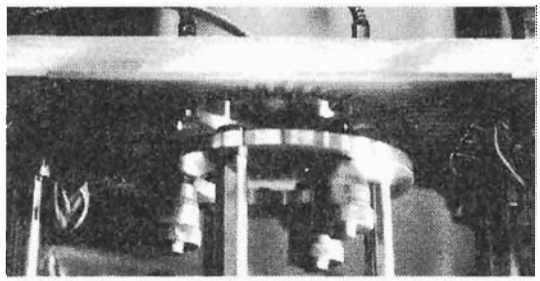

Fig. 15 Photograph showing rotor under stable suspension in ESIM (rotor is made of ITO layered glass)

a photograph of the ITO layered disk under stable suspension.

Rotation was enabled by supplying three-phase ac voltages of 1 kV p-p to the electrodes-for-rotation after a stable suspension was reached. We have succeeded in rotating the ITO layered glass disk with a maximum speed of 70 rpm. As in ESVCM, the maximum attainable rotor speed was limited by the lateral restriction forces.

Fig. 16 shows the gap length and voltage variations at a

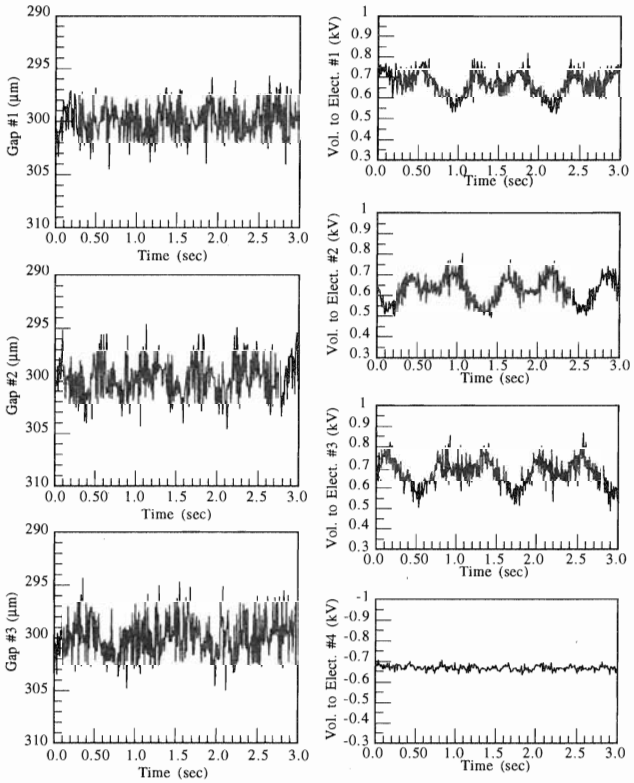

Fig. 16 Gap and voltage variations during rotation in ESIM (rotor is made of ITO layered glass)

rotor speed of 50 rpm. Gap fluctuations did not exceed 5 μm p-p while the voltage fluctuations supplied to electrodes #1, #2, #3 and #4 were 0.21 kV, 0.19 kV, 0.2 kV, 0.04 kV, respectively.

Next, the suspension and rotation experiments were carried out with the glass disk having no surface treatment. A bias voltage of 0.78 kV is supplied to electrode #1, #2 and #3, and -0.78 kV to electrode #4. Since glass is a material having a

high resistivity, a certain period of time is needed to accumulate sufficient induced charges on the glass surface facing the electrodes-for-suspension for picking up the rotor. Fig. 17 shows the gap length and voltage variations after the PID compensator was switched on. It shows that a period of time of approximately 1 minute was needed for the glass disk to actually reach a state of suspension. This period of time is strongly dependent on the environmental humidity. The data shown in Fig. 17 was recorded under an air humidity of 42

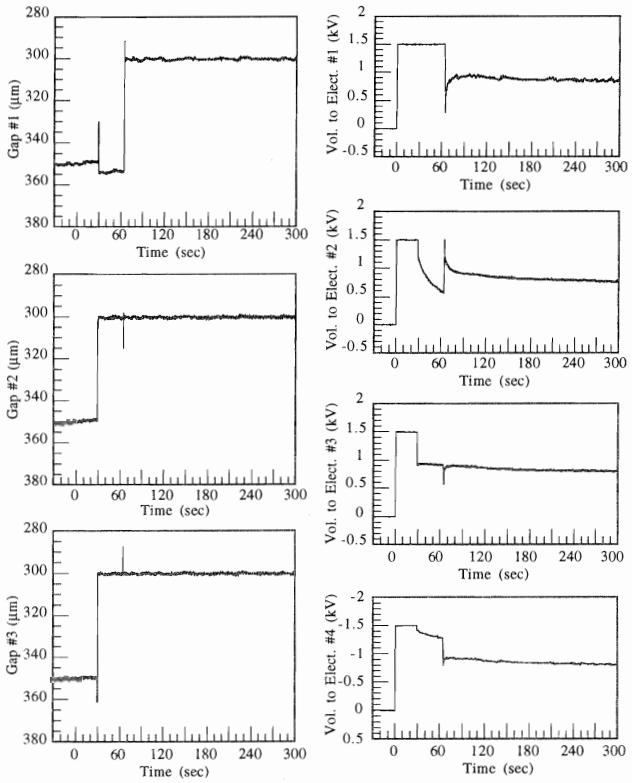

Fig. 17 Gap and voltage variations during levitation process in ESIM (rotor is glass disk without any surface treatment)

%RH. From our experiments, it was observed that the period of time needed to achieve a stable suspension varied from 30 seconds to 3 minutes for a humidity variation from 50 %RH to 30 %RH. Fig. 17 also shows that during the state of stable suspension, the actively controlled voltages are slowly decreasing. A physical explanation for this drift phenomenon is that the charge built-up on the glass surface had not yet reached a steady state, consequently, the process of charge accumulation was progressing continuously during suspension.

Rotation experiments were conducted by supplying three-phase ac voltages of 1 kV p-p to the electrodes-for-rotation. The maximum achievable speed was 30 rpm, which is smaller compared with the case of the ITO layered glass disk. The reason is that the lateral movement of the glass disk without any surface treatment reveals a hysteretic-like characteristic so that in the event of an lateral disturbance, the disk does not return back to its original position after removing the disturbance.

The ESIM is an asynchronous motor. Nevertheless, it was observed that the rotor speed was synchronous to the frequency of the supplied voltage. The reason for this is that the torque produced by ESIM is large enough to overcome the external torques which is caused only by air friction since the rotor is suspended.

4 Conclusions

Two types of electrostatic rotary actuators with a function of contactless electrostatic suspension, which are electrostatically suspended variable-capacitance motors (ESVCM) and electrostatically suspended induction motors (ESIM), were described in this paper. Both motor types feature stator electrodes which are subdivided into a part responsible for suspension and one for rotation. In ESVCM, a disk on which an electrode pattern is formed was used as rotor. In ESIM, two rotor types were utilized: a glass disk covered with a thin layer of conductive material (ITO layer) on only one side, and a glass disk without any surface treatment. In both motor types, the rotors have been suspended successfully at a gap length of 300 μm by actively controlling the electrostatic forces acting on it. While being suspended stably, the rotor was rotated with a rotational speed of approximately 60 rpm. The gap fluctuations were found to be no greater than 6 μm during rotation. The proposed actuators is expected to be widely used in industrial applications as a positioning and rotating mechanism.

Acknowledgement

The authors thank S. J. Woo for his help in preparing this paper.

References

[1] T. Higuchi, A. Horikoshi and T. Komori, "Development of an Actuator for Super Clean Rooms and Ultra High Vacua", *Proc. 2nd Int. Symp. Magnetic Bearings*, Tokyo, Japan, pp.115-122, July 1990.

[2] S. F. Bart, T. A. Lober, R. T. Howe, J. H. Lang and M. F. Schlecht, "Design Considerations for Micromachined Electric Actuators", *Sensors and Actuators*", Vol. 14, pp. 269-292, 1988.

[3] S. Kumar, D. Cho and W. N. Carr, "Experimental Study of Electric Suspension for Microbearings", *J. Microelectromechanical Systems*", Vol. 1, No. 1, pp. 23-30, March 1992.

[4] J. Jin, T. Higuchi and M. Kanemoto, "Electrostatic Silicon Wafer Suspension", *Proc. 4th Int. Symp. Magnetic Bearings*, ETH Zurich, Switzerland, pp. 343-348, August 1994.

[5] B. Bollee, "Electrostatic Motors", *Philips Technical Review*, Vol. 30, No. 6/7, pp. 178-194, 1969.

[6] T. Niino, T. Higuchi and S. Egawa, "Dual Excitation Multiphase Electrostatic Drive", *Proc. 30th IAS Annual Meeting*, Florida, USA, Vol. 2, pp. 1318-1325, Oct. 1995.

[7] S. D. Choi and D. A. Dunn, "A Surface-Charge Induction Motor", *Proc. IEEE*, Vol. 59, No. 5, pp. 737-748, 1971.

[8] S. J. Woo, J. U. Jeon, T. Higuchi and J. Jin, "Electrostatic Force Analysis of Electrostatic Levitation System", *Proc. 34th SICE Annual Conf.*, International Session, Hokkaido, Japan, pp. 1347-1352, July 1995.